Biol. Cybern. 84, 183–192 (2001)

Biological Cybernetics

Statistical characteristics of climbing fiber spikes necessary for efficient cerebellar learning

Shinya Kuroda[1,2,*], **Kenji Yamamoto**[3,**], **Hiroyuki Miyamoto**[1], **Kenji Doya**[1,4], **Mitsuo Kawato**[1,3]

[1] Kawato Dynamic Brain Project, ERATO, Japan Science and Technology Corporation, 2-2, Hikaridai, Seika-cho, Soraku-gun, Kyoto 619-0288, Japan
[2] Division of Signal Transduction, Nara Institute of Science and Technology, Ikoma 630-0101, Japan
[3] ATR, Human Information Processing Research Laboratories, 2-2, Hikaridai, Seika-cho, Soraku-gun, Kyoto 619-0288, Japan
[4] Information Science Division, ATR international and CREST, Japan Science and Technology Corporation, 2-2, Hikaridai, Seika-cho, Soraku-gun, Kyoto 619-0288, Japan

Received: 28 January 2000 / Accepted in revised form: 2 August 2000

Abstract. Mean firing rates (MFRs), with analogue values, have thus far been used as information carriers of neurons in most brain theories of learning. However, the neurons transmit the signal by spikes, which are discrete events. The climbing fibers (CFs), which are known to be essential for cerebellar motor learning, fire at the ultra-low firing rates (around 1 Hz), and it is not yet understood theoretically how high-frequency information can be conveyed and how learning of smooth and fast movements can be achieved. Here we address whether cerebellar learning can be achieved by CF spikes instead of conventional MFR in an eye movement task, such as the ocular following response (OFR), and an arm movement task. There are two major afferents into cerebellar Purkinje cells: parallel fiber (PF) and CF, and the synaptic weights between PFs and Purkinje cells have been shown to be modulated by the stimulation of both types of fiber. The modulation of the synaptic weights is regulated by the cerebellar synaptic plasticity. In this study we simulated cerebellar learning using CF signals as spikes instead of conventional MFR. To generate the spikes we used the following four spike generation models: (1) a Poisson model in which the spike interval probability follows a Poisson distribution, (2) a gamma model in which the spike interval probability follows the gamma distribution, (3) a max model in which a spike is generated when a synaptic input reaches maximum, and (4) a threshold model in which a spike is generated when the input crosses a certain small threshold. We found that, in an OFR task with a constant visual velocity, learning was successful with stochastic models, such as Poisson and gamma models, but not in the deterministic models, such as max and threshold models. In an OFR with a stepwise velocity change and an arm movement task, learning could be achieved only in the Poisson model. In addition, for efficient cerebellar learning, the distribution of CF spike-occurrence time after stimulus onset must capture at least the first, second and third moments of the temporal distribution of error signals.

Correspondence to: M. Kawato
(Tel.: +81-774-95 1058, Fax: +81-774-95 1008
e-mail: kawato@hip.atr.co.jp)
Present addresses:
*Center for Neurobiology and Behavior,
Columbia University, 1051 Riverside Drive,
New York, NY 10032, USA
**Neuroscience section, Electrotechnical Laboratory,
Ibaraki 305-8568, Japan

1 Introduction

The cerebellum has been shown to play a pivotal role in motor learning (Ito 1984). Cerebellar Purkinje cells (PCs), the only efferent neurons in cerebellar cortex, receives two major afferents: multiple parallel fiber (PF) inputs encoding the sensori-motor context to PCs, and a single climbing fiber (CF) input encoding the error signals for learning (Kitazawa et al. 1998; Kobayashi et al. 1998). The CF inputs have been postulated to be essential for modifying the PF-PCs synapses in a supervised-learning manner, resulting in an acquisition of cerebellar representation of the inverse model (Kawato 1999).

Cerebellar synaptic plasticity has been shown to provide the biological basis of cerebellar learning (Ito 1989). Several types of synaptic plasticity have been found in PCs: long-term depression (LTD) (Ito 1989), long-term potentiation (LTP) (Sakurai 1987; Hirano 1990), and rebound potentiation (RP) (Kano et al. 1992; Kano 1996). Cerebellar LTD is a process of a decrease in the synaptic weights between PFs and PCs induced by the conjunctive stimulation of PFs and CFs (Ito 1989). LTP has been shown to be induced presynaptically by the stimulation of PFs in the absence of CF stimulation (Hirano 1990; Sakurai 1987). PCs also receive inputs from inhibitory cells (ICs) in the molecular layer, in addition to PFs (Kano et al. 1992; Kano 1996). RP is a process of an increase in the synaptic weights between

ICs and PCs induced by the conjunctive activation of ICs and PCs. Computational models that replicate learning of eye and arm movement tasks based on these synaptic plasticity mechanism have been proposed (Schweighofer et al. 1998; Yamamoto et al. 1998a,b).

Mean firing rates (MFRs), with analogue values, have thus far been used as information carriers of neurons in most theories of cerebellar motor learning (Kawato and Gomi 1992). We have shown that cerebellar motor learning, including an acquisition of ocular following response (OFR) (Yamamoto et al. 1998a,b), a slow eye movement with a short latency (Miles and Kawano 1986), and an arm movement task (Schweighofer et al. 1998), can be reproduced using MFR as the error signal of CFs. However, real neurons transmit the signal by spikes, which are discrete events. It is not obvious whether learning is possible with discrete spike trains. Even worse, CFs have been shown to fire at ultra-low rates (around 1 Hz). We have already found experimentally that, despite the ultra-low firing rates of CFs, the temporal firing patterns of CFs carry high-frequency information and a smooth waveform when many trials of OFR are averaged (Kobayashi et al. 1998). However, it remains to be demonstrated, on a theoretical basis, how this temporal averaging is carried out and how motor learning can be achieved by CF spikes.

To address this issue we performed a computer simulation of cerebellar learning using CF spikes – instead of MFR – as the error signal for PCs. Four spike models were examined in accordance with the MFR as follows: (1) a Poisson model in which the spike interval probability follows a Poisson distribution, (2) a gamma model in which the spike interval probability follows the gamma distribution, (3) a max model in which a spike is generated when an input reaches a maximum, and (4) threshold model in which a spike is generated when the input crosses a certain small threshold. The Poisson and gamma models are stochastic, while the max and threshold models are deterministic. OFR and arm movement tasks were used to test the spike models. Furthermore, we analyzed the statistical characteristics of spikes of CFs required for efficient cerebellar learning.

2 Methods

In this study the OFR task and the arm movement task were used to examine whether models using CF spikes were capable of reproducing the efficient cerebellar motor learning.

2.1 Acquisition of the ability to control OFR and the gain adaptation of visuo-motor transformation

The OFR is the tracking of movement of the eye evoked by the movements of a visual scene, and is thought to be important for the visual stabilization of gaze (Miles and Kawano 1986). We have built a mathematical model that reproduces OFR based on electrophysiological experiments (Yamamoto et al. 1997). We have formulated the generalized linear models which can reconstruct well the temporal firing patterns of CFs during the OFR of monkeys (Kobayashi et al. 1998). Based on these results, we have shown (K. Yamamoto, Y. Kobayashi, A. Takemura, K. Kawano, M. Kawato, in preparation) that acquisition and adaptation of the OFR can be reproduced by the computational model of the OFR, including the synaptic plasticity of cerebellar cortex (Yamamoto et al. 1998a,b). In the study reported here, we built the computational model which reproduces the vertical OFR based on the previous model (Fig. 1). In the block diagram of the OFR shown in Fig. 1, we replaced the MFR of the CF, $C(t)$, by the spikes generated by the spike generation models as below, in order to examine whether cerebellar learning can be achieved using spikes instead of the MFR.

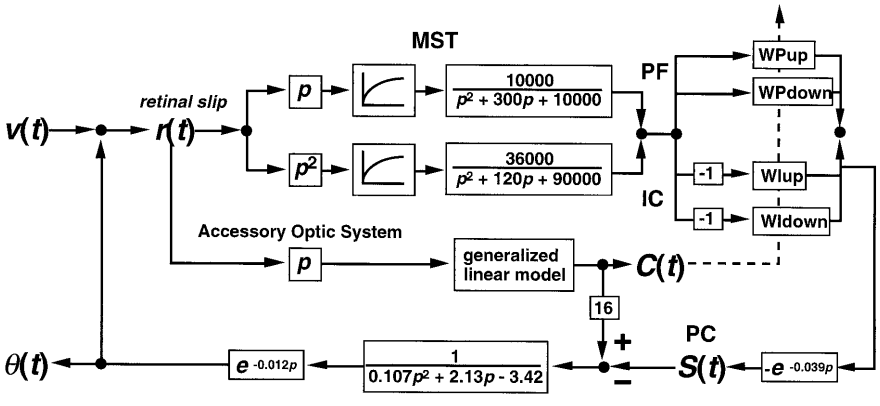

Fig. 1. Block diagram of the ocular following response (OFR) control. $v(t)$: the visual stimulus at time t; $r(t)$: the retinal slip at time t; $s(t)$: signal of simple spike at time t; $\theta(t)$: the position of eye at time t; $c(t)$: signal of CF at time t; *PC*: Purkinje cell; *PF*: parallel fiber; *IC*: inhibitory cell; *MST*: medial superior temporal area; p: Laplace operator; *WPup*: synaptic weights between PF whose preferred direction is upward and PCs; *WPdown*: synaptic weights between PF whose preferred direction is downward and PCs; *WIup*: synaptic weights between IC whose preferred direction is upward and PCs; *WIdown*: synaptic weights between IC whose preferred direction is downward and PCs

Two tasks for the OFR were chosen: (1) the acquisition of the ability to control OFR after birth, by ramp trials in which the vertical visual stimuli whose velocities were constant were given; and (2) gain adaptation for a visuo-motor transformation using speed-step trials in which the vertical visual stimuli whose velocities was changed in a stepwise-manner were given (Miles and Kawano 1986). There are two types of speed-step trials: the step-up stimuli whose velocities were increased in a stepwise-manner and the step-down stimuli whose velocities were decreased in a stepwise-manner. The ramp and speed-step stimuli for the simulation of the OFR were reconstructed based on the stimuli used in the previous physiological experiment (Kobayashi et al. 1998). For the simulation of the acquisition of the ability to control the OFR, upward and downward ramp stimuli were given 8750 times (Yamamoto et al. 1998a,b). For the gain adaptation of the visuo-motor transformation, upward step-down and downward step-up stimuli were given 875 times. In each trial the gain, given by the maximum eye velocity divided by the maximum visual velocity, was recorded. We evaluated the cerebellar learning during these tasks by the gain.

LTD, LTP and RP were modeled as three known classes of synaptic plasticity in PCs for cerebellar learning (Yamamoto et al. 1998a,b). When PFs and CFs, or ICs and CFs simultaneously fire, LTD or RP occurs at the respective synapses. When PFs or ICs fire without CF firing, LTP or no change of synaptic efficacy occurs at the respective synapses. The strength of the synaptic plasticity induction was dependent on the time interval between the stimulation of PFs or ICs, and that of CFs. The time interval between these stimulations, known as the time window, has been analyzed in detail (Karachot et al. 1994). We have already made a re-interpretation of their results and produced the time window which follows a Gaussian distribution with a mean of −100 ms and a standard deviation at 50 ms for the simulation of OFR (Yamamoto et al. 1998a,b). In this study we used the same time window. That is, LTD becomes most effective when the PF stimulation precedes the CF stimulation by 100 ms. Based on the time window and the synaptic plasticity, we built the learning rule by which the synaptic weights between PFs and the PC are modified as follows.

$$\eta(t) = \int_0^t PF(t)G(t'-t)\mathrm{d}t'$$

$$\dot{w}(t) = -\frac{1}{\tau}(w(t)-w_0) - \frac{1}{n_{\mathrm{LTD}}}\eta(t)l(CS(t)-CS_{\mathrm{sp}}) + \frac{1}{n_{\mathrm{LTP}}}\eta(t)l(CS_{\mathrm{sp}}-CS(t))$$

where,

$$l(x) = \begin{cases} 0 : x < 0 \\ x : x \geq 0 \end{cases}$$

In this equation, $w(t)$ denotes the synaptic transmission efficacy at time t. w_0 denotes the initial value of the synaptic transmission efficacy, and was set at 0.2. The first term denotes the forgetting factor. The second and third terms denote the changes induced by LTD and LTP, respectively. $PF(t)$ and $CS(t)$ denote the firing rates of PF and the occurrence of CF spikes at time t, respectively. CS_{sp} denotes the spontaneous firing rates of the CF (1 Hz). $G(t)$ is the integral kernel. $G(t'-t)$ is given by the Gaussian distribution as described above. n_{LTD} and n_{LTP} are the coefficients of LTD and LTP, respectively, and were set at 8.5066×10^4 and 3.7807×10^4, respectively. τ, the time constant of the forgetting factor was set at 4.67×10^3 according to Miles and Kawano (1986). Synaptic weights were modified off-line by the above equation after each trial.

Similarly, the synaptic weights between the ICs and the CFs were modified by the above equation except that $PF(t)$ denotes the firing rates of ICs instead of that of PFs, w_0 was set at −0.2, n_{RP} was used instead of n_{LTD}, and the coefficient in the third term was set to zero because synaptic weight is not affected by the IC stimulation in the absence of that of the CF (Kano 1996).

2.2 Two-link arm movement

In addition to the OFR, two-link arm movement was used in this study (Kawato et al. 1987; Miyamoto et al. 1988) (Fig. 2). A planar point-to-point arm reaching movement with a 500-ms duration was used. The workspace was set within an annulus whose radius was between 30 and 90% of the arm length from the center

Table 1. Moments of the temporal distribution of the error signals of CFs in the ocular following response (OFR) ramp trials in each model

	Direction	Mean firing rates	Poisson	Gamma $n = 50$	Max	Threshold
First moment	Upward	105.9	107.5	105.9	97.8	30.8
	Downward	92.0	88.1	87.1	51.7	73.9
Second moment	Upward	2.75e+3	2.81e+3	2.66e+3	0.778e+3	0.257e+3
	Downward	3.81e+3	3.96e+3	3.44e+3	0.00146e+3	2.49e+3
Third moment	Upward	−0.0153	−0.0810	−0.0202	0.382	−0.951
	Downward	0.156	0.211	0.287	1.23	−0.403
Fourth moment	Upward	2.00	2.07	2.03	4.96	1.95
	Downward	1.66	1.64	1.84	2.68	1.56
Fifth moment	Upward	−0.241	−0.611	−0.307	10.3	−2.90
	Downward	0.634	0.841	1.27	4.78	−0.855

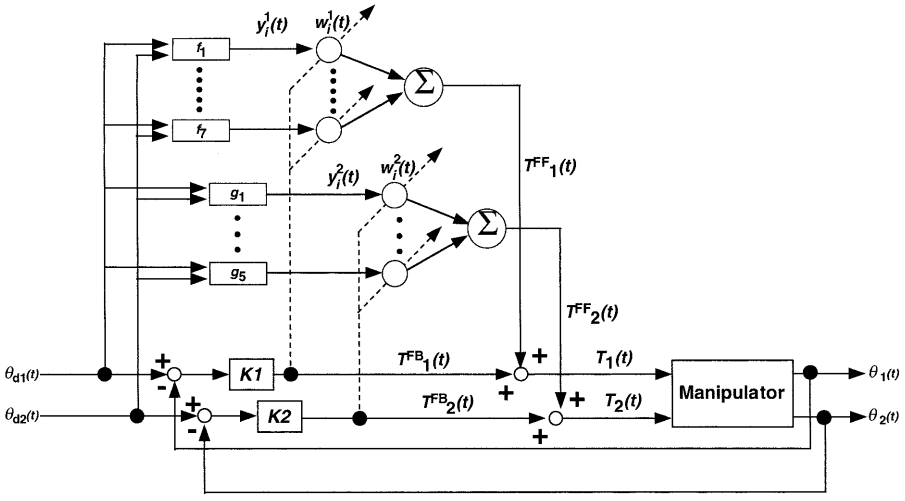

Fig. 2. Block diagram of the control of the two-link arm movement. $\theta_{dj}(t)$: the desired joint angle of the arm at time t; $\theta_j(t)$: the real joint angle of the arm at time t; *manipulator*: the artificial two-link arm; $T_j^{FF}(t)$: feedforward torque generated by the inverse dynamics model at time t; $T_j^{FB}(t)$: the feedback torque at time t; $T_j(t)$: the torque for the regulation of the manipulator at time t; K_j: the feedback gains. Here, K_j was set at 60. $w_i^j(t)$: synaptic weight between ith PF and PCs responsible for the jth joint; $y_i^j(t)$: ith PF signal responsible for the regulation of jth joint; g_i: ith nonlinear subsystem responsible for the control of the elbow joint; i: the index of the nonlinear subsystems; j: the index of the joint, shoulder or elbow. Nonlinear functions of the subsystems responsible for the control of shoulder and elbow joints are $\ddot{\theta}_{d1}$, $\ddot{\theta}_{d1}\cos\theta_{d2}$, $\ddot{\theta}_{d2}\cos\theta_{d2}$, $\dot{\theta}_{d2}$, $\dot{\theta}_{d1}\dot{\theta}_{d2}\sin\theta_{d2}$, $\dot{\theta}_{d2}^2\sin\theta_{d2}$ and $\dot{\theta}_{d1}$, and $\ddot{\theta}_{d1}\cos\theta_{d2}$, $\ddot{\theta}_{d1}$, $\ddot{\theta}_{d2}$, $\dot{\theta}_{d1}\sin\theta_{d2}$ and $\dot{\theta}_{d2}$, respectively

of the shoulder (Nakano et al. 1999). The initial and final hand positions were randomly selected within the workspace. Hand trajectories have been known to be preplanned as desired trajectories before the movement without on-line correction (Kawato 1999). Many computational models on how hand trajectories are planned have been proposed (Kawato 1999). In this study, the minimum hand jerk model was used for trajectory planning (Flash and Hogan 1985). The inputs of the desired trajectory, $\theta_{dj}(t)$, were fed to nonlinear subsystems and were nonlinearly transformed into n different PF signals, $y_i^j(t)$ $(i = 1, \ldots, n; j = 1, 2)$ (Kawato et al. 1987; Miyamoto et al. 1988) (Fig. 2). $w_i^j(t)$ denotes a synaptic weight of the ith inputs into the jth PC. The output signal, $T_j^{FF}(t)$, was given by the sum of $y_i^j(t)$ weighted by $w_i^j(t)$ as follows:

$$T_j^{FF}(t) = \sum_{i=1}^{N_j} w_i^j(t) y_i^j(t)$$

The feedback torque, $T_j^{FB}(t)$, was generated based on the error signal given by the difference between the desired trajectory, $\theta_{dj}(t)$, and the real trajectory, $\theta_j(t)$ (Miyamoto et al. 1988). The manipulator receives the torque, $T_j(t)$, which is the sum of $T_j^{FF}(t)$ and $T_j^{FB}(t)$, and outputs the resulting trajectory, $\theta_j(t)$ (Kawato et al. 1987; Miyamoto et al. 1988). Since $T_j^{FB}(t)$ encodes the error signal of the trajectory, $T_j^{FB}(t)$ was used as the error signal to generate CF spikes. We assume that the synaptic weight, $w_i^j(t)$, was changed off-line according to following equation after each trial:

$$\tau \dot{w}_i^j(t) = -y_i^j(t) T_j^{FB}(t)$$

Here, τ is a time constant of changes of the synaptic weights and was set at 9.6375×10^3. The efficiency of learning is evaluated by the mean square error (MSE) in the last 100 trials as given by the difference between the real synaptic weights and the desired synaptic weights with which the desired trajectory is executed.

2.3 Spike generation models

To generate the spikes based on the MFR of the CF, we built the following spike models: (1) a Poisson model in which the spike interval probability follows a Poisson distribution, (2) a gamma model in which the spike interval probability follows the gamma distribution, (3) a max model in which a spike is generated when the CF reaches maximum, and (4) a threshold model in which a spike is generated when the CF input crosses a certain small threshold. In each model, the time step was 1 ms.

A spike in the Poisson model was generated by the following equation:

$$C(t) = \begin{cases} 1: \ \text{input}(t) > \text{rand}(t) \\ 0: \ \text{input}(t) \leq \text{rand}(t) \end{cases}$$

$C(t)$ and input(t) denote the CF spikes and the MFR of the CF at time t, respectively rand(t) is a random number uniformly distributed between 0 and 1, selected at time t.

A spike in the gamma model was generated by the following equation:

$$n(t) = \begin{cases} n(t-1) + 1 & : \ \text{input}(t)\text{m} > \text{rand}(t) \\ n(t-1) & : \ \text{input}(t)\text{m} \leq \text{rand}(t) \end{cases}$$

$$C(t) = \begin{cases} 1: n(t) = m \\ 0: n(t) < m \end{cases}$$

m denotes the order of the gamma model. $n(t)$ is an internal counter which is set randomly between 1 and m at the beginning of a trial. Once a spike fires, $n(t)$ is reset to zero.

In the Poisson and gamma models, a spike was generated on-line with a 1-ms time step. We examined the behaviour of gamma models with orders of 4, 50, 100, and 200. Since the gamma model with order 50 showed the best ability for cerebellar learning among these gamma models, we used this model.

A spike in the max model was generated by first detecting the time, t_2, when the MFR of the CF first reaches a maximum, and then deciding off-line whether a spike fires or not by the following equation:

$$C(t_2) = \begin{cases} 1: \text{Inputs} > \text{rand} \\ 0: \text{Inputs} \leq \text{rand} \end{cases}$$

$C(t_2)$ and Inputs denote the CF spikes at time t_2 and the sum of the MFRs of the CF in each trial, respectively.

A spike in the threshold model was generated off-line in a similar manner, except that t_2 denotes the time 3 ms after the MFR of the CF become different from its spontaneous rate.

All the parameters in each spike model were set so that the total spike numbers in each model were almost the same.

2.4 Measurement of moments of the spike array

To analyze the statistical characteristics of the spike model, the stimulus-triggered spike histogram was regarded as a probability distribution over a time bin of 1 ms. Thus, the P_i is given by the number the spikes at the time t_i divided by the total number of spikes accumulated over all time and trials. On the other hand, the random variable t_i is the spike occurrence time after stimulus onset. This set of the random variable and the probability (t_i, P_i) gives a probability distribution of spike occurrence time. We measured the moments of the probability distribution in each spike model, and analyzed the statistical characteristics. The first moment, α_1, and the second moment, α_2, are the mean and the variance of the firing time, respectively. The nth moment, α_n, is computed by the following equation. As with the spike models, the moments of the MFR model are also computed with a 1-ms time step.

$$\alpha_1 = \sum_{i=1}^{T} tP_i = \mu$$

$$\alpha_2 = \sum_{i=1}^{T} (t-\mu)^2 P_i = \sigma^2$$

$$\alpha_n = \sum_{i=1}^{T} \frac{(t-\mu)^n P_i}{\sigma^n}$$

where n denotes an integer greater than or equal to 3. t and T denote the firing time and the duration of each trial, respectively. μ is α_1, the mean of firing time, and σ is the square root of the variance of the spike array, α_2.

3 Results

3.1 Comparison of the spike models with the MFR model in the acquisition of the ability to control OFR after birth

We performed the computer simulation of the acquisition of the ability to control OFR after birth with ramp stimuli 17500 times. In the MFR model, the synaptic transmission efficacy became stable by the repetition of the ramp trials. The OFR gain increased adaptively in the upward and downward 10-deg/s trials, and became almost one (Fig. 3a,f). In the Poisson and gamma models similar results were obtained (Fig. 3b,g and Fig. 3c,h respectively). In the max model, the OFR gain in the upward ramp trials (after the trials) were almost the same as those of the MFR, the Poisson, and the gamma models (Fig. 3d). However, the OFR gain in the downward ramp trials diverged (Fig. 3i). In the threshold model, the OFR gain in the upward ramp trials did not increase (Fig. 3e), and that in the downward ramp trials diverged as well as in the max model (Fig. 3j).

To understand how gain is acquired by the CF spikes, we compared the temporal distribution of the spike array in the spikes models with the firing rates of the MFR model. In the upward ramp trials of the MFR model, firing rates increased during the period between 50 ms and 200 ms after the onset of the ramp trials (Fig. 3k). As well as in the MFR model, in the Poisson and gamma models spike arrays were observed during the period between 50 ms and 200 ms after the onset (Fig. 3l,m). In the max model, although the firing time of spikes were relatively clustered, the spike array was observed during the period (Fig. 3n). The spikes during the period between 50 ms and 200 ms led to the changes of the synaptic transmission efficacies between PFs and ICs, and PCs by the induction of LTD and RP, respectively, indicating that the changes of the synaptic transmission efficacy are responsible for the acquisition of the OFR gain. In contrast, in the threshold model no spike was observed during the period between 50 ms and 200 ms, due to the immediate response of spikes after the onset of the ramp trials (Fig. 3o). The absence of spikes during this period led to the induction of LTP but not to LTD or RP, resulting in the failure of the acquisition of the OFR gain.

In the downward ramp trials, the firing rates decreased during the period between 50 ms and 200 ms in the MFR model (Fig. 3p). Similarly, the decrease of the spike arrays was observed during this period in the Poisson and the gamma models (Fig. 3q,r). The decrease of the spike arrays led to the changes of the synaptic transmission efficacy between PF and PCs by the induction of LTP, indicating that the changes of synaptic transmission efficacy are responsible for the acquisition of the OFR gain. In the max and the threshold models, the decrease of the spike arrays was also observed during

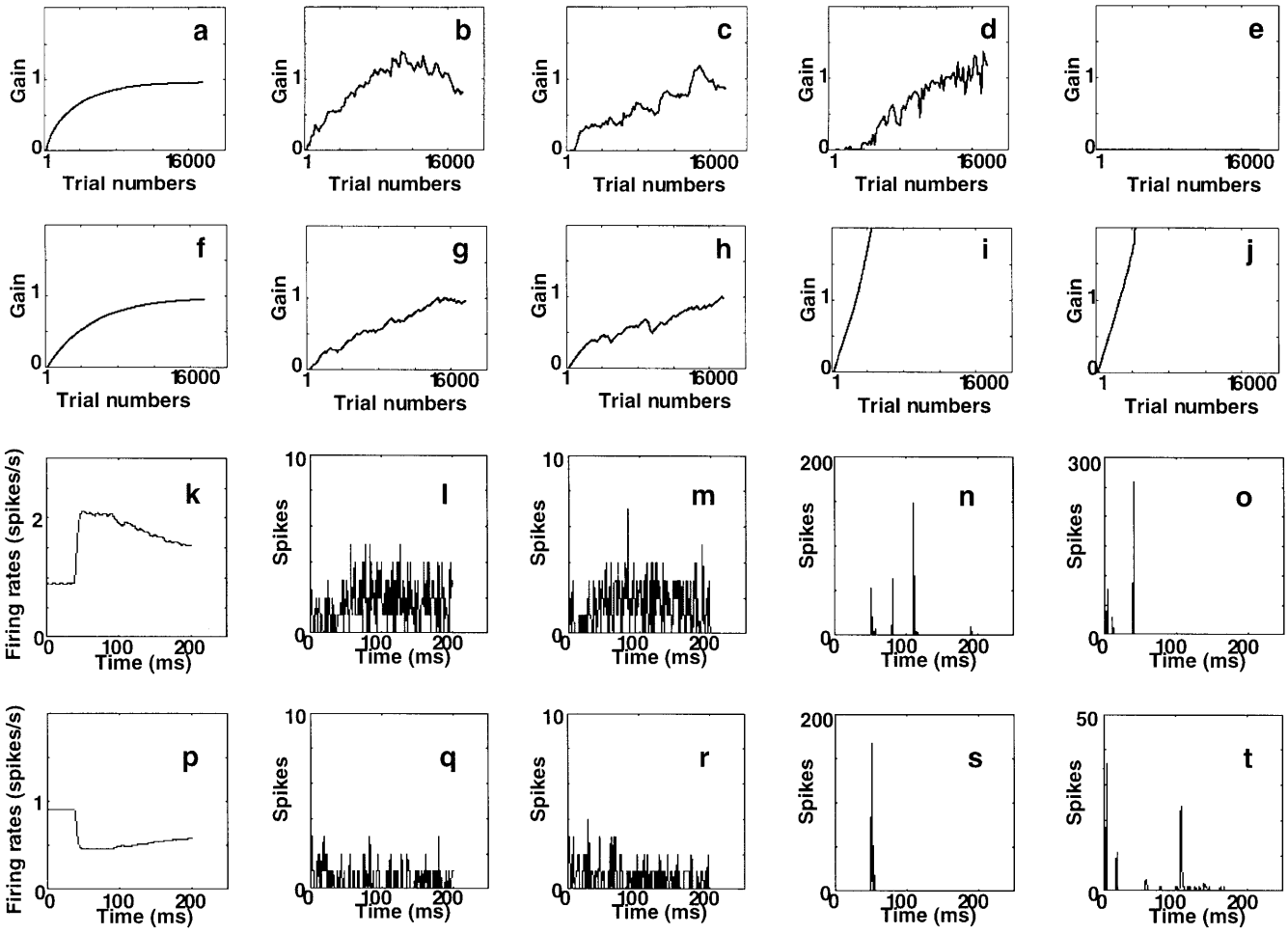

Fig. 3a–t. The changes of the gain in the OFR ramp trials and the accumulated CF spikes over all ramp trials in each model. **a–j** the changes of the gain in the OFR ramp trials: **a–e** the changes of the gain in the upward 10-deg/s trials; **f–j** the changes of the gain in the downward 10-deg/s trials; **a,f** the mean firing rate (MFR) model; **b,g** the Poisson model; **c,h** the gamma model; **d,i** the max model; **e,j** the threshold model. **k–t** the accumulated CF spikes over all ramp trials in each model; **k–o** the accumulated CF spikes over all upward ramp trials; **p–t** the accumulated CF spikes over all downward ramp trials; **k,p** the MFR model; **l,q** the Poisson model; **m,r** the gamma model; **n,s** the max model; **o,t** the threshold model

this period (Fig. 3s,t). However, the numbers of spikes during this period were much less than in the MFR, the Poisson, and the gamma models, so that LTP became too strong, resulting in the divergence of the eye movement by the strong increase of the OFR gain.

To analyze the statistical characteristics of the temporal distribution of spike arrays that are required for the efficient cerebellar learning, we measured the moments of the temporal distribution of spikes in each spike model. In the upward ramp trials, the OFR underwent adaptation in the MFR, the Poisson, the gamma, and the max models, whereas the OFR did not in the threshold model. The first moment of the spike array in the threshold model was different from those in others (Table 1). In the downward ramp trials, the OFR underwent adaptation in the MFR, the Poisson, and the gamma models, whereas the OFR did not in the max and the threshold models. The first moment of the spike array of the max model differed from those of the MFR, the Poisson, and the gamma models. In the threshold model, the second and the higher moments differed from those of the MFR, the Poisson, and the gamma models. These results suggest that at least the first and second moments of the spike array of CFs should be the same as those in the MFR models for the acquisition of the ability to control the OFR.

3.2 Comparison of the spike models with the MFR model in a gain adaptation for a visuo-motor transformation

In the MFR, the Poisson, and the gamma models, the OFR underwent adaptation in both of the upward and downward trials. Using these three models, we next performed the simulation of the gain adaptation for a visuo-motor transformation using upward and downward speed-step trials repeated 1750 times. In the MFR model, the gain increased adaptively in the downward step-up trials (Fig. 4a). In the upward step-down trials, the gain decreased adaptively (Fig. 4d). In the Poisson model, the gains adaptively increased and decreased in the step-up and step-down trials, respectively (Fig. 4b,e).

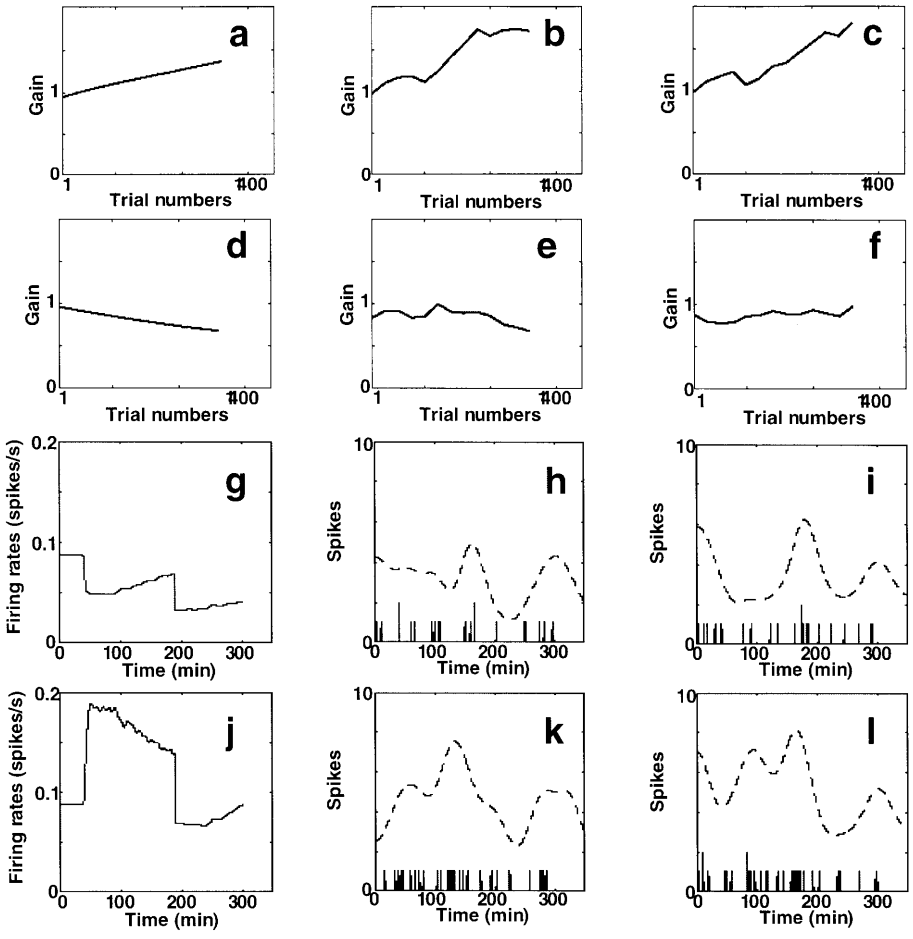

Fig. 4a–l. The changes of the gain in the OFR speed-step trials and the accumulated CF spikes over all speed-step trials in each model. **a–f** the changes of the gain in the OFR speed-step trials: **a–c** the changes of the gain in the downward step-up (10–100 deg/s) trials; **d–f** the changes of the gain in the upward step-down (10–0 deg/s) trials; **a,d** the MFR model; **b,e** the Poisson model; **c,f** the gamma model. **g–l** the accumulated CF spikes over all speed-step trials in each model; **g–i** the accumulated CF spikes over all downward step-up trials; **j–l** the accumulated CF spikes over all upward step-down trials; **g,j** the MFR model; **h,k** the Poisson model; **i,l** the gamma model. *Dashed line* denotes the moving average weighted by a Gaussian distribution with a 20-ms standard deviation

In the gamma model, the gain increased adaptively in the step-up trials (Fig. 4c). However, the gain did not decrease in the step-down trials (Fig. 4f).

We next analyzed the temporal distribution of the spike arrays and the synaptic plasticity induced by the spike arrays. In the MFR model, the firing rates kept decreasing during 300 ms after the onset of the step-up trials (Fig. 4g). The decrease in firing rates during the first 150 ms induced LTP but did not affect the OFR because the LTD had already balanced with the diminishing effect in the previous ramp trials, and thereby synaptic transmission efficacy did not largely change. However, the decrease in firing rates lasted further during the last 150 ms, leading to the changes of the synaptic transmission efficacy by the induction of LTP (Fig. 4g). The changes of the synaptic transmission efficacy resulted in the gain adaptation of the OFR. In the Poisson and the gamma models as well, the decrease of the numbers of spikes during the last 150 ms led to the induction of LTP and thereby the gain increased adaptively (Fig. 4h,i). In the step-down trials, the firing rates increased during the first 150 ms in the MFR, resulting in the induction of LTD, but this LTD did not affect the OFR because LTD had already balanced with the forgetting factor in the previous ramp trials. The decrease in firing rates during the last 150 ms led to the changes of the synaptic transmission efficacy by the induction of LTP (Fig. 4j), resulting in the adaptive decrease of the OFR gain. In the Poisson model, the decrease in the numbers of spikes during the last 150 ms led to the induction of LTP and thereby the gain decreased adaptively (Fig. 4k). In contrast, in the gamma model, the numbers of the spikes during the last 150 ms did not decrease (Fig. 4l), so that the synaptic transmission efficacy did not change largely because of the absence of LTD or RP, resulting in the failure of the adaptation of the OFR gain.

We measured the moments of the temporal distribution of the spike arrays in each model that are required for the efficient cerebellar learning in the speed-step trials. In the step-up trials, the OFR underwent adaptation in all of the models tested. However, in the step-down trials, the OFR underwent adaptation in the MFR and the Poisson models, whereas the OFR did not in the gamma model. In the step-down trials, the third moment in the gamma model was different from those in others (Table 2). These results suggest that the temporal distribution of the spike arrays should encode the third moment of the temporal distribution of the error signal in the step-down trials.

3.3 Comparison of the spike models with the MFR model in the point-to-point reaching two-link arm movement

We performed the simulation of the point-to-point reaching arm movement 200 000 times using the MFR,

Table 2. Moments of the temporal distribution of the error signals of CFs in the OFR speed-step trials in each model

	Speed-step	Mean firing rates	Poisson	Gamma
First moment	Step-down	133.0	146.3	121.9
	Step-up	129.4	139.2	143.0
Second moment	Step-down	5.94e+3	6.42e+3	5.23e+3
	Step-up	7.42e+3	8.07e+3	8.81e+3
Third moment	Step-down	0.420	0.277	0.194
	Step-up	0.258	0.262	0.173
Fourth moment	Step-down	2.28	2.04	2.09
	Step-up	1.94	1.97	1.79
Fifth moment	Step-down	2.08	1.11	1.57
	Step-up	1.27	1.08	0.502

the Poisson, the max, and the threshold models. We evaluated the learning in an arm movement task by the MSEs between the desired and the actual synaptic weights of each joint in the last 100 trials. Repetition of the point-to-point reaching arm movement task rendered the MSEs stable after the 200 000 trials. After 5000 trials, the MSE of the synaptic weights of the PFs and PCs responsible for the control of the shoulder joint in the MFR, Poisson, max, and threshold models were 0.0484, 0.0531, 0.0548, and 0.0629, respectively. The MSE of the synaptic weights responsible for the control of the elbow joint in the MFR, Poisson, max, and threshold models were 0.0218, 0.0245, 0.0251, and 0.0452, respectively. MSEs in the Poisson and the max model, as well as in the MFR model, rapidly decreased, whereas the MSEs slowly decreased in the threshold model. After the 200 000 trials, when the MSEs in each model became very small and converged, the MSEs of the synaptic weights of the PFs and PCs responsible for the control of the shoulder joint in the MFR, Poisson, max, and threshold models were 0.0061, 0.0041, 0.3175, and 0.0197, respectively. The MSEs of the synaptic weights responsible for the control of the elbow joint in the MFR, Poisson, max, and threshold models were 0.0020, 0.0023, 0.1658, and 0.0242, respectively. In the max model, although the MSEs decreased rapidly at the beginning of the trials, the MSEs did not become small or converge. The MSEs in the threshold model did not become small or converge either. Thus, the MFR and the Poisson models enabled the efficient cerebellar learning in the arm movement task, whereas the max and the threshold models did not.

We measured the moments of the temporal distribution of the spike arrays in each model in the arm movement task (Table 3). In comparing the moments of the spike arrays encoding the positive error signal of the shoulder in each model, the first moment in the threshold model differed from those in the MFR and the Poisson models. The third moment in the max model, but not the first and second moments, largely differ from those in the MFR and the Poisson models (Table 3). Similar results were obtained in the spike arrays encoding the negative error signal of the shoulder and the

Table 3. Moments of the temporal distribution of the positive error signals of CFs responsible for the control of the shoulder joint in the two-link arm movement

	Mean firing rates	Poisson	Max	Threshold
First moment	298.3	306.0	321.5	12.3
Second moment	1.70e+3	1.57e+3	2.18e+3	1.76e+3
Third moment	−0.240	−0.274	−0.0464	5.76
Fourth moment	1.92	1.92	1.39	37.98
Fifth moment	−1.25	−1.25	−0.158	267.7

error signal of the elbow. Therefore, it is likely that the temporal distribution of the spike arrays should encode at least the third moment of the temporal distribution of the error signal in the arm movement task.

4 Discussion

In this study we examined whether cerebellar learning can be achieved using the spikes by which neurons transmit the signal, instead of using the conventional MFR. In the ramp trials and the step-down trials, the OFR underwent adaptation in the Poisson and the gamma models, in addition to the MFR. In contrast, cerebellar learning was achieved in the step-down trials and in the two-link arm movement only in the Poisson model. These results indicate that cerebellar learning can be achieved using the spikes of the error signals of CFs instead of the MFR.

What kind of statistical characteristics of spikes are important for efficient cerebellar learning? In the upward ramp trials the OFR underwent adaptation in the Poisson, the gamma, and the max models, but not in the threshold model. The failure in the threshold model is due to the different changes of the synaptic transmission efficacy in the threshold model from those in others: LTD and RP occurred in the Poisson, the gamma, and the max models, whereas LTP occurred in the threshold model. This difference comes from the distinct temporal distributions between the threshold model and the other models. The first moment of the temporal distribution of the spike array in the threshold model was largely different from those in other models. Thus, it is likely that the temporal distribution of the spike array should encode the first moment of the error signal in the upward ramp trials. In addition, the second and third moments of the temporal distribution of the spike array in the threshold model also differed from those in the MFR, the Poisson, and the gamma models. In the max model, although the first moment of the temporal distribution of the spike array did not largely differ from those in the MFR, the Poisson, and the gamma models, the second and higher moments were largely different. The reason why the cerebellar learning can be achieved in the max model despite the fact that the second and higher moments were largely different from those in the other models, is due to the time window used in the OFR trials. Without the time window, the eye movement had to diverge in the max model because LTD and RP would

occur too strongly by the direct effect of the spikes together with the inputs from the PFs. Since the time window used here followed a Gaussian distribution with a mean of −100 ms and a standard deviation of 50 ms, the effect of the spikes became relatively weak and, consequently, the OFR underwent adaptation.

In the downward ramp trials, learning was successful in the Poisson and the gamma models, whereas the learning could not be achieved in the max and the threshold models. The changes of the synaptic transmission efficacy in all of the models were the same: they were induced by LTP. However, since no or very few spikes fired in the max and the threshold models during the period between 50 ms and 200 ms, LTP was induced too strongly and, as a consequence, the eye movements diverged. In the max model, the first and higher moments of the temporal distribution of the spike array were different from those in the other models. In the threshold model, the second and higher moments were different. These results suggest that the temporal distribution of the spike array have to encode at least the first and second moments of the error signal for efficient cerebellar learning.

Among the simulation of the speed-step trials of the OFR, learning could be achieved in all the models in the step-up trials. However, in the step-down trials, learning was successful in the MFR and the Poisson models, whereas learning could not be achieved in the gamma model. In the step-down trials, LTD and RP were induced in the MFR and the Poisson models. However, synaptic plasticity was not induced in the gamma model. In both step-up and step-down trials, the first and second moments of the temporal distribution of the spike arrays were almost the same among the models, but the third moment of the temporal distribution of the spike array in the gamma model was different from those in the other models. Why then, in the gamma model, could learning be achieved in the step-up trials and but not in the step-down trials? In the step-up trials, firing rates kept decreasing during the first 300 ms after the onset. In contrast, in the step-down trials, the firing rates increased during the first 150 ms and decreased during the last 150 ms. Since the firing time of the spikes tends to be delayed by the waiting time in the gamma model, the temporal distribution of the spike array becomes relatively right-shifted compared to the MFR and the Poisson models. Therefore, the number of the spikes in the gamma model did not decrease during the last 150 ms in the step-down trials, due to the effect of the right-shifted temporal distribution of the spike array, resulting in the failure of the decreased gain adaptation. This right-shift of the temporal distribution of the spike array appears as the difference in the third moment between the gamma models and the other models. Therefore, in the case of the stimulus in which the firing rates of the error signal fluctuates across the spontaneous firing rates such as in the step-down trials, the temporal distribution of the gamma model becomes right-shifted due to the effect of the waiting time, resulting in the failure of cerebellar learning. This result also suggest that the temporal distribution of the spike array should encode the third moment of the temporal distribution of the error signals in the step-down trials.

In the point-to-point reaching arm movement task, learning could be achieved in the MFR and the Poisson models, but not in the max and the threshold models. At the early stages of the trials, the MSEs rapidly decreased in the Poisson and the max model. However, in the later stages of the trials when the MSEs in all the models converged, the MSEs in the MFR and the Poisson models were very small, whereas the MSEs in the max and the threshold models were relatively high. In the max model, since a spike fires when the maximal value of the input of the error signal is given, LTD occurred too strongly compared to in the MFR and the Poisson models and, as a consequence, the MSEs became relatively large. In comparing with the moments in each spike models, the first, third, and higher moments of the temporal distribution of the spike array in the threshold were different from those in the MFR and the Poisson models. In the max model, although the first and second moments were not largely different, the third moment was largely different. Thus, it is likely that the temporal distribution of the spike array should encode at least the first, second, and third moments of the temporal distribution of the error signals in the step-down trials. Moreover, since the firing rates of the error signals fluctuates across the spontaneous firing rates in the arm movement task as well as in the step-down trials in the OFR, it seems important that the temporal distribution of the spike array encodes the third moment of the temporal distribution of the error signals.

Taken together with the results of the OFR and the arm movement task, it seems important that the temporal distribution of the spike array encodes the first and second moments – but not the third moment – of the temporal distribution of the error signals in the trials in which the firing rates of the error signals constantly increase or decrease, such as in the ramp trials and the step-up trials in the OFR. In contrast, in the trials in which the firing rates of the error signals fluctuates across spontaneous rates, the third moment of the temporal distribution of the spike array seems important for efficient cerebellar learning. In conclusion, it is likely that the temporal distribution of the spike array should encode at least the first, second, and third moments of the temporal distribution of the error signals for cerebellar learning. Among the spike models tested here, only the Poisson model can satisfy the statistical characteristics required for efficient cerebellar learning.

The Poisson and the gamma models share the similar characteristics because a spike fires randomly in an input-dependent manner. In contrast, in the max and threshold models, a spike fires totally in an input-dependent manner. Thus, the former two models can be regarded as stochastic, while the latter two models are deterministic. In this study, on a theoretical basis we demonstrated that efficient cerebellar learning can be achieved only when a spike fires in a stochastic manner. Does the temporal distribution of the spikes of CFs share the similar characteristics as the Poisson model? It has been shown that the spikes of CFs fire randomly in

behaving animals at rest (Keating and Thach 1995). Furthermore, we have already found that the spikes of CFs also fire randomly during the OFR in Monkeys (Kobayashi et al. 1998). These observations are consistent with our results. The inferior olive neurons, the source of the CF inputs to cerebellar PCs, have been shown to have extensive electrical coupling with each other through gap junctions (De Zeeuw et al. 1995). Based on this finding, we computationally simulated small networks of electrically coupled inferior olive neurons, combined with non-linear ionic currents (Schweighofer et al., 1999; N. Schweighofer, K. Doya, J. Chiron, H. Fukai, M. Kawato, in preparation). We found that the electrical coupling, together with the non-linear ionic currents, resulted in the irregular and stochastic firing of CFs. This stochastic characteristic of CF firing enhanced the input-output mutual information, and thereby efficient cerebellar learning can be achieved despite the ultra-low firing rates of CFs. Taken together, efficient cerebellar learning requires stochastic firing of CF spikes in an input-dependent manner.

Acknowledgement. S.K. thanks Drs. K. Kaibuchi and H. Qadota (NAIST, Japan) for their encouragement.

References

De Zeeuw CI, Hertzberg EL, Mugnaini E (1995) The dendritic lamellar body: a new neuronal organelle putatively associated with dendrodendritic gap junctions. J Neurosci 15: 1587–1604

Flash T, Hogan N (1985) The coordination of arm movements: an experimentally confirmed mathematical model. J Neurosci 5: 1688–1703

Hirano T (1990) Depression and potentiation of the synaptic transmission between a granule cell and a Purkinje cell in rat cerebellar culture. Neurosci Lett 119: 141–144

Ito M (1984) The Cerebellum and Neural Control. Raven, New York

Ito M (1989) Long-term depression. Ann Rev Neurosci 12: 85–102

Kano M (1996) Long-lasting potentiation of GABAergic inhibitory synaptic transmission in cerebellar Purkinje cells: Its properties and possible mechanism. Behav Brain Sci 19: 354–361

Kano M, Rexhausen U, Dreessen J, Konnerth A (1992) Synaptic excitation produces a long-lasting rebound potentiation of inhibitory synaptic signals in cerebellar Purkinje cells. Nature 356: 601–604

Karachot L, Kado RT, Ito M (1994) Stimulus parameters for induction of long-term depression in in vitro rat Purkinje cells. Neurosci Res 21: 161–168

Kawato M (1999) Internal models for motor control and trajectory planning. Curr Opin Neurobiol 9: 718–727

Kawato M, Gomi H (1992) A computational model of four regions of the cerebellum based on feedback-error learning. Biol Cybern 68: 95–103

Kawato M, Furukawa K, Suzuki R (1987) A hierarchical neural-network model for control and learning of voluntary movement. Biol Cybern 57: 169–185

Keating JG, Thach WT (1995) Nonclock behavior of inferior olive neurons: interspike interval of Purkinje cell complex spike discharge in the awake behaving monkey is random. J Neurophysiol 73: 1329–1340

Kitazawa S, Kimura T, Yin PB (1998) Cerebellar complex spikes encode both destinations and errors in arm movements. Nature 392: 494–497

Kobayashi Y, Kawano K, Takemura A, Inoue Y, Kitama T, Gomi H, Kawato M (1998) Temporal firing patterns of Purkinje cells in the cerebellar ventral paraflocculus during ocular following responses in monkeys II. Complex spikes. J Neurophysiol 80: 832–848

Miles FA, Kawano K (1986) Short-latency ocular following responses of monkey. III. Plasticity. J Neurophysiol 56: 1381–1396

Miyamoto H, Kawato M, Setoyama T, Suzuki R (1988) Feedback-error-learning neural network for trajectory control of a robotic manipulator. Neural Netw 1: 251–265

Nakano E, Imamizu H, Osu R, Uno Y, Gomi H, Yoshioka T, Kawato M (1999) Quantitative examinations of internal representations for arm trajectory planning: minimum commanded torque change model. J Neurophysiol 81: 2140–2155

Sakurai M (1987) Synaptic modification of parallel fibre-Purkinje cell transmission in in vitro guinea-pig cerebellar slices. J Physiol (Lond) 394: 463–480

Schweighofer N, Doya K, Kawato M (1999) Electrophysiological properties of inferior olive neurons: A compartmental model. J Neurophysiol 82: 804–817

Schweighofer N, Spoelstra J, Arbib MA, Kawato M (1998) Role of the cerebellum in reaching movements in humans. II. A neural model of the intermediate cerebellum. Eur J Neurosci 10: 95–105

Yamamoto K, Kobayashi Y, Takemura A, Kawano K, Kawato M (1997) A mathematical model that reproduces vertical ocular following responses from visual stimuli by reproducing the simple spike firing frequency of Purkinje cells in the cerebellum. Neurosci Res 29: 161–169

Yamamoto K, Kobayashi Y, Takemura A, Kawano K, Kawato M (1998a) A computational simulation on the adaptation of vertical ocular following responses. Tech Rep IEICE NC97-131: 229–236

Yamamoto K, Takemura A, Kawano Y, Kobayashi Y, Kawato M (1998b) Computational simulation of transformation from visual inputs into motor command during ocular following responses. Tech Rep IEICE NC98-29: 37–44